Preparation of a sludge-based adsorbent and adsorption of dimethyl phthalate from aqueous solution

Zhihui Pan*, Bin Huang, Chaosheng Zhang

Ministry of Education and Guangdong Province Key Laboratory for Water Quality Security and Protection in Pearl River Delta, Guangzhou University, No. 230, Wai Huan Xi Road, Guangzhou Higher Education Mega Center, Guangzhou 51006, P.R. China, Tel./Fax: +86 20 39366657; emails: ri13@163.com (Z. Pan), 371659073@qq.com (B. Huang), gdzcs@126.com (C. Zhang)

ABSTRACT

In this paper, a sludge-based adsorbent (SBA) was prepared from biochemical sludge from a wastewater treatment plant by chemical activation using 3.0 M $ZnCl_2$ followed by pyrolysis at 700°C for 1 h in an anoxic atmosphere. The physical and chemical properties of the SBA were characterized by N_2 adsorption, scanning electron microscopy (SEM), Fourier Transform infrared red (FT-IR) spectroscopy, X-ray diffraction (XRD), and Boehm titrations. The adsorption behavior of dimethyl phthalate (DMP) on the SBA was studied in batch reactors by investigating a range of variables including pH, DMP concentration, and adsorption time. The optimal pH for DMP adsorption was found out to be around 6, as this gave the best surface charge interactions. Adsorption equilibrium isotherms and the kinetics models of DMP adsorption on the SBA were also investigated. Experimental data indicated that the Freundlich model was most applicable to the adsorption process to show the SBA's heterogeneous surface supporting sites of varied affinities with DMP. In addition, the adsorption kinetics of DMP on SBA was described by the pseudo-second-order kinetic model suggesting that the chemical adsorption was the predominant rate-limiting stage of the adsorption process. It was demonstrated that the SBA is a low-cost promising and highly effective product for removal of DMP from aqueous solutions. The effectiveness of the SBA can be explained in terms of the π-electron interactions, electrostatic interactions, and H-bonding interactions contributing its high adsorption capacity.

Keywords: Sludge-based adsorbent; Adsorption; Dimethyl phthalate; Kinetics; Equilibrium isotherm

1. Introduction

Phthalic acid esters (PAEs) are widely used as plasticizers in the plastics, ceramics, paper, cosmetics, ink, and paint industries [1]. Among these PAEs, dimethyl phthalate (DMP) is the most widely employed compound in our daily necessities. Due to its high mobility in the aquatic system, DMP is easily leached from the solid products and detected in almost all parts of our environment such as soil, water, and atmosphere, even in wildlife and humans [2,3]. Another major concern is that the DMP is a class of endocrine disrupting chemicals which have the ability to invade the human body and play the role of the hormone estrogen [4]. It is harmful to reproductive

*Corresponding author.

development, and has thus threatened the health and safety of animals and humans beings [5]. Moreover, it is reported that the contaminant is related to the birth defects, organ damage, infertility, and cancer. Hence, the China National Environmental Monitoring Centre, the European Union, and USA Environmental Protection Agency (EPA) have categorized the majority of PAEs, including DMP, as priority pollutants [6].

The most common method for PAEs removal is biological treatment, based on the metabolic degradation of PAEs by microorganisms [7,8]. However, this method has relatively low removal efficiency and it requires long processing time [4]. Other investigations have also been conducted on physicochemical methods for PAEs removal, including photodegradation [9], catalytic ozonation [10,11], UV/TiO$_2$ [12], light-assisted fenton [13], electrochemically assisted coagulation [14], and adsorption techniques [15–17]. Among these methods, adsorption is an approach specifically appropriate for the removal of the toxic organic compounds in wastewater due to its low dissolubility and highly hydrophobic character of PAEs. Successful DMP adsorption was noticed through the use of activated carbon or modified materials from aqueous solution. Wang et al. studied the effects of DMP adsorption and desorption on five types of carbon nanotubes [2]. Huang et al. indicated that compared with the raw material, the octadecyl-modified mesoporous SBA-15 silica molecular sieves have higher capacities for DMP adsorption [18].

It has been considered that sewage sludge, a byproduct produced in large volumes in wastewater treatment processes, requires an efficient and environmentally friendly approach for its utilization. In addition, biochemical sludge is carbonaceous in nature, and so has a potential for use as an adsorbents; it not only provides an eco-friendly alternative for the adsorption of pollutants, such as heavy metals, acidic gases, and organic compounds [19], but also a way to recycle the sludge produced in the treatment processes.

Although several researchers have reported successful DMP adsorption or other PAEs using commercial activated carbon [20–22], to our knowledge so far, no systematic studies have been conducted to investigate the DMP adsorption onto the adsorbent derived from sewage sludge in the aqueous environments. Therefore, this study aims to develop appropriate preparation method of adsorbents derived from sewage sludge in wastewater plants, and to evaluate the effectiveness of sludge-based adsorbent (SBA) for the toxic organic material (DMP) removal from aqueous solution. In addition, the authors will also further investigate physical and chemical characterizations of SBA, isotherm, and kinetic models and pH effect for DMP adsorption and the interaction between DMP and SBA.

2. Materials and methods

2.1. Materials and regents

The sewage sludge (SS) used for SBA preparation in this study was the byproduct of aerobic biological treatment of activated sludge from a wastewater treatment plant located in Taishan (Guangdong Province, China). All reagents in the experiments were of analytic grade and used without further purification.

2.2. Preparation and characterization of SBA

2.2.1. Preparation

The dewatered SS sample (water content was 70%) was initially dried at 105°C for 24 h to reduce water content to <5%. The dried SS was then ground and sieved to obtain a powder with the diameter <0.1 mm, and impregnated in an activating agent (3.0 M ZnCl$_2$) with a mass ratio of 1:1. Under mechanical stirring at 30°C, the mixtures of SS and ZnCl$_2$ were maintained contact in the air for 24 h, and subsequently dried at 105°C in air for a further 24 h. Pyrolysis of the SS was then carried out in a muffle furnace under anaerobic conditions, while the temperature was increased to 700°C at a rate of 15°C/min, and the final temperature of 700°C was maintained for 1 h. The resulting product was ground and sieved to a powder of approximately 0.1 mm and washed with 3.0 M HCl to remove acid-soluble inorganic contaminants [23,24]. The sample was then washed repeatedly with deionized water until the pH of the supernatant liquid became constant (close to neutral). Finally, the sample was dried at 105°C over 24 h.

2.2.2. Characterization

To investigate the surface morphology characteristics of the SBA, the samples were observed by scanning electron microscopy (SEM) (SEM, JSM-6490LV, JEOL). Textural characterization was obtained from N$_2$ adsorption isotherms at −196°C with a surface area analyzer (ASAP 2020, Micromeritics). Before N$_2$ adsorption, the samples were outgassed at 150°C for 3 h under vacuum (P/P_0 range: 0.0562–0.191) to remove all moister and gases from the surface and pores of samples. The specific surface area (S_{BET}) was calculated by Brunauer–Emmett–Teller (BET) method. Micropore volume (V_{mic}) was obtained by t-plot

method. Mesopore and macropore volume ($V_{mes + mac}$) were calculated by Barrette–Joyner–Halenda (BJH) method. Average pore diameter (D_p) and pore size distribution were obtained by Horvath–Kawazoe (HK) method [25].

The pH at the point of zero charge (pH$_{PZC}$) was determined by titration method [26]. The fixed carbon, volatile and ash contents (proximate analysis) of SS and SBA were measured by the standard test method [27] and the carbon, hydrogen, and nitrogen compositions (ultimate analysis) of SS and SBA were obtained by elemental analysis (R48-VarioEL III, Elementar). The quantities of surface acidic functional groups (carboxyl, lactone, phenolic hydroxyl, and carbonyl) on the SBA were calculated by using Boehm titration method described in previous reported paper [28]. The elemental contents of heavy metals in the SS and SBA were measured by an Inductively Coupled Plasma Atomic Emission Spectroscopy (ICP-AES, Plasma 1000, Pekin Elmer Inc). Before the analysis, the samples were digested by soaking 0.5 g of each sample in the mixtures of 6 ml HCl and 2 ml HNO$_3$ at 180°C for 45 min in a microwave digestion device (Mars-6 CEM, USA). In order to determine the quantities of metals leached from SBA, the adsorbent (10.0 g) were soaked in 100 mL of deionized water (pH 7.0) and stirred at 150 rpm for 24 h. The metals concentrations in the resultant leachate were then analyzed ICP–AES. To determine the surface functional groups, FT-IR spectroscopy (Aratar 370, Thermo electron) using the potassium bromide pellet method was carried out [29]. The crystal structures of the adsorbent were analyzed by a powder X-ray diffraction (XRD) (XRD, D/max-2500, Rigaku) with monochromatic Cu Kα radiation (45 kV, 50 mA).

2.3. Adsorbate

A DMP stock solution was prepared by dissolving DMP (1.0 g) in deionized water (1.0 L) and allowing the solution to equilibrate for 24 h with constant stirring, to ensure sufficient dissolution. The physical and chemical properties of DMP are shown in Table 1.

The DMP concentration was detected by high performance liquid chromatography (HPLC, Agilent 1200 Infinity), using a methanol water (80:20, v/v) mobile phase at a flow rate of 1.0 mL/min, a DMP detection wavelength of 230 nm.

2.4. Adsorption experiment

2.4.1. Effect of pH on DMP adsorption

Batch experiments were conducted to study the effects and mechanisms of DMP adsorption at initial pH values 2–10. These initial pH values were obtained by the addition of NaOH (0.1 M) or HCl (0.1 M) solutions. Adsorption experiments were performed by immersing portions of the SBA (4 g/L) into DMP solutions (100 mL of 1,000 mg/L) in 250 mL conical flasks, and shaking the samples for 2 h at 30°C in a vapor-bathing constant temperature vibrator (SHZ-82A, Shunhua Instrument Co., China). The equilibrium time and optimal SBA dosage are determined to be 2 h and 4 g/L, respectively. To obtain the liquid supernatant and minimize interference of the SBA particles during the analysis, the samples were centrifuged for 1 min at 4,000r/min upon equilibration. The DMP uptake (q_t) was calculated according to Eq. (1):
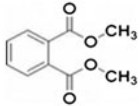
$$q_e = \frac{(C_0 - C_e)V}{W} \qquad (1)$$

where q_e is the quantity (mg/g) of DMP adsorbed at equilibrium, C_0, C_e, and V are the initial concentration (mg/L), final concentration (mg/L), and volume (L) of the adsorbate solution, respectively, while W is the weight (g) of the SBA used.

2.4.2. Adsorption isotherms modeling

Throughout the study, the DMP concentration was varied from 50 to 1,000 mg/L at constant SBA feed of 4 g/L. To study the SBA adsorption capacity of DMP,

Table 1
Physical and chemical properties of DMP

Chemical	Structure	Molecular weight (g/mol)	pK_a	Solubility (mg/L)	Configuration
Dimethyl phthalate (DMP)		194.19	8.59, 11.3	4,200	not planar

the classical models applied to equilibrium adsorption isotherms, namely the Langmuir (Eq. (2)) and Freundlich (Eq. (3)) isotherm models, were investigated.

$$\frac{C_e}{q_e} = \frac{1}{q_m}C_e + \frac{1}{K_L q_m} \qquad (2)$$

$$\ln q_e = \frac{1}{n}\ln C_e + \ln K_f \qquad (3)$$

where C_e (mg/L) is the adsorbed equilibrium concentration of adsorbate, q_e (mg/g) is the quantity adsorbed per gram of adsorbent at equilibrium, q_m (mg/g) is the maximum adsorption capacity with monomolecular adsorbent surface assumption, K_L (L/mg) is the Langmuir equilibrium constant. K_f (L/g) is the Freundlich constant related to the adsorption capacity of the adsorbent and n is a constant associated with sorption intensity. The Langmuir isotherm constants (q_m, K_L) and the Freundlich isotherm constants (K_f, n) can be calculated from the intercept and slope of the liner plots obtained from Eqs. (2) and (3), respectively.

2.4.3. Adsorption kinetics modeling

To investigate the SBA adsorption mechanism, the pseudo-first-order (Eq. (4)) and, pseudo-second-order (Eq. (5)) adsorption kinetic models, along with the intraparticle diffusion (Eq. (6)) were used to fit the experimental kinetic data.

$$\ln(q_e - q_t) = -K_1 t + \ln q_e \qquad (4)$$

$$\frac{t}{q_t} = \frac{1}{q_e}t + \frac{1}{K_2 q_e^2} \qquad (5)$$

$$q_t = K_p t^{0.5} + A \qquad (6)$$

where q_t and q_e are the quantities adsorbed per gram of adsorbent (mg/g) at contact time t and at equilibrium, respectively. K_1 is the rate constant of pseudo-first-order adsorption (min), while K_2 is the rate constant of the pseudo-second-order adsorption (g/(mg min)), and K_p is the intraparticle diffusion constant (mg/(g min)). In addition, $t^{0.5}$ is the square root of the time t, and A is the intercept concerned with the thickness of the boundary layer. The first-order rate constant (K_1, q_e), the second-order rate constant (K_2, q_e), and the intraparticle diffusion constant (K_p, A) can be calculated from the intercept and slope of the liner plots obtained from Eqs. (4)–(6), respectively.

3. Results and discussion

3.1. Adsorbent characterization

3.1.1. Physical characterization

The surface morphology images of SS and the SBA obtained from SEM analysis (5,000× magnification) are shown in Fig. 1. It is clear from the SEM images that the surface morphology was altered significantly following pyrolysis. The surface structure of SS was smooth with little obvious pore structure. However, following activation by $ZnCl_2$, a rough SBA surface was observed, covered with deeper grooves and pores of different size and shapes. This indicated that the SBA may exhibit improved adsorption over SS.

Table 2 shows the carbon textural properties obtained from nitrogen adsorption isotherm data. The S_{BET} of the SBA was 316.24 m²/g, which is significantly greater than that of SS (3.56 m²/g). This was
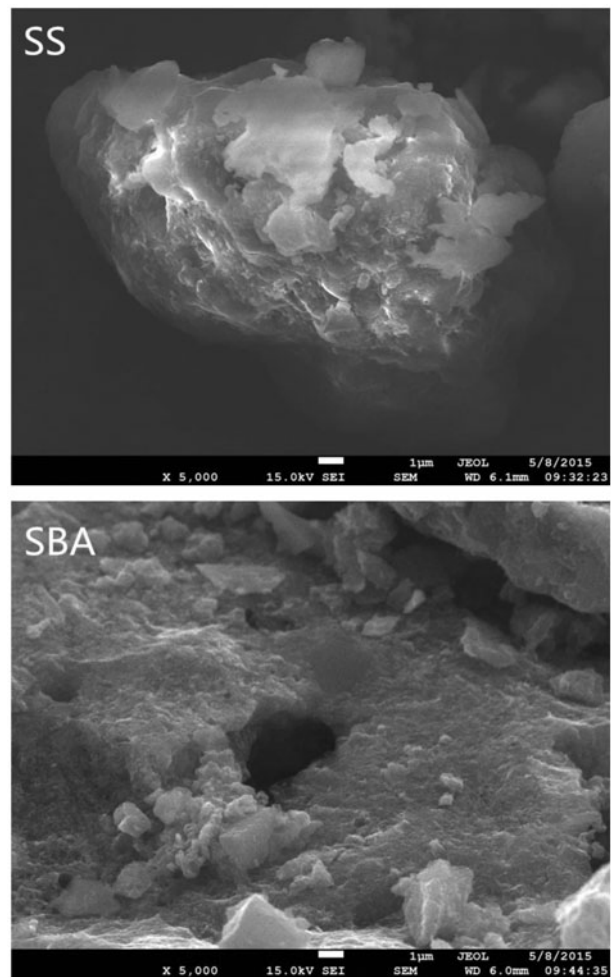

Fig. 1. SEM of SS and SBA.

Table 2
Surface area and porosity of SS and SBA

	V_{mic} (cm^3/g)	$V_{mes + mac}$ (cm^3/g)	S_{BET} (m^2/g)	D_p (nm)
SS	–	0.05	3.56	–
SBA	0.07	0.17	316.24	1.15

mainly due to the cautery effect of ZnCl$_2$ on the carbon matrix and the volatile release of the sewage sludge for creating pores during pyrolysis [30].

The N$_2$ adsorption–desorption isotherm of the SBA is shown in Fig. 2(a). The resulting adsorption–desorption isotherms showed a hysteresis loop which was considered to be a typical type IV isotherm following the classification of BDDT [31]. Moreover, the isotherm showed a sharp knee at low relative pressures ($P/P_0 < 0.05$) suggesting that SBA is microporous, while a gradual increase at higher P/P_0 values ($P/P_0 > 0.1$) indicates the presence of well-developed mesoporosity. It is therefore expected that the porous

Fig. 2. (a) N$_2$ adsorption–desorption isotherms and (b) pore size distribution of SBA.

structures on the SBA surface may contribute to its excellent adsorption capacity.

The pore size distribution of the SBA is illustrated in Fig. 2(b). The pore volume was mainly distributed in the micropore range of 7–21 Å. Moreover, an intense peak in the 8–10 Å pore diameter range also indicated the presence of narrow micropores. The pore diameter may affect the transport of molecules into the SBA pores, and therefore influence the adsorption capacity for organic substances with different molecular diameters. As can be seen in Table 2, the average pore diameter of the SBA was 11.5 Å, which is in the micropore range. However, the macro- and mesopore volume (0.17 cm^3/g) was significantly greater than that of the micropores (0.07 cm^3/g), indicating that the SBA possesses a remarkable affinity with low molecular diameter adsorbates.
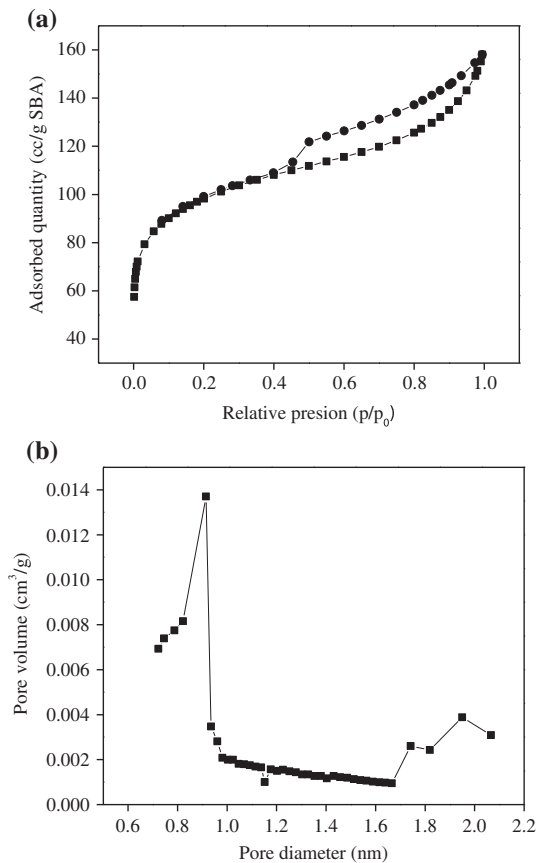
3.1.2. Chemical characterization

The proximate and ultimate analysis corresponding to the SBA and its raw material SS are shown in Table 3. The low carbon and high ash contents of the raw material (28.0 and 48.1%, respectively) might lead to the relatively low BET surface area of SBA (shown in Table 2) compared to the majority of commercial activated carbons (400–1,500 m^2/g) [32]. However, the resulting product generated from SS was enriched, and exhibited significantly higher carbon content (37.6%) and lower ash amount (22.0%) than its precursor. In contrast, after the activation, the hydrogen and nitrogen contents of the sample decreased from 6.86 to

Table 3
Proximate analysis and ultimate analysis of SS and SBA

		SS	SBA
	pH$_{pzc}$	–	5.9
Proximate analysis (wt%)	Ash	48.1	22
	Volatiles	38.8	33.8
	Fixed carbon	13	44.2
Ultimate analysis (wt%)	Carbon	28	37.6
	Hydrogen	6.86	1.28
	Nitrogen	5.63	4.04

1.28% and 5.63 to 4.04%, respectively. This indicated that dehydrogenative polymerization and dehydrative polycondensation existed during activation and heat treatment [33].

The surface acidic functional groups contents on the SBA calculated by the Boehm titration method are shown in Table 4. As can be seen in Table 4, the main acidic functional groups concentrations varied according to the following sequence: Carbonyl (0.527 mmol/g) > lactone (0.397 mmol/g) > carboxyl (0.185 mmol/g) > phenolic hydroxyl (0.098 mmol/g). The presence of the hydroxyl moieties within carboxylic and phenolic hydroxyl groups might therefore facilitate the adsorption capacity of the SBA through surface interactions with adsorbates. The mechanisms for this process are discussed further in Section 3.5.

Table 5 shows the contents of five selective heavy metals in the SS and SBA and their leachate concentrations from the SS and SBA. It can be seen that the concentration of Zn increased greatly in SBA in comparison with the precursor material (SS). It might be that the adsorbent had affinity for activating agent $ZnCl_2$ adsorption or the elemental metal was bound up with the adsorbent structure during activation. Other heavy metals had also been enriched in the SBA because of volatile releasing from SS during pyrolysis (shown in Table 3) [34]. However, it was found that only slight leaching characteristics of heavy metals from the SBA, which might be attributed to the thorough washing procedure. The low heavy metals leaching from the SBA indicated that the adsorbent material would be satisfied with safety standard for most industrial wastewater treatment.

The FT-IR spectrum shown in Fig. 3 demonstrates the existence of a number of surface functional groups on the SBA. The broad bands at 3,500 and 3,300 cm^{-1} were in accordance with the −OH stretching vibration, likely pertaining from the phenolic, hydroxylic, and carboxylic moieties. An additional strong band at approximately 1,600 cm^{-1} corresponded to the C=O stretching vibrations [34]. Furthermore, an intense peak between 1,100 and 1,000 cm^{-1} was observed, likely corresponding to Si–O–Si or Si–O–C stretching vibrations, implying that the SBA contained a certain quantity of mineral matter [35]. Thus, the presence of –OH, C=O and Si–O–Si/Si–O–C functional groups on the SBA, indicated that it has the potential to uptake

Table 4
Contents of surface acidic functional groups of SBA

	Carboxyl	Lactone	Phenolic hydroxyl	Carbonyl
SBA	0.185	0.397	0.098	0.527

Table 5
Contents of metals (mg/kg) in the SS and SBA and Leaching metals amount (µg/g) from SS and SBA

	Zn	Pb	As	Cr	Cu
SS	985.3	118.7	8.72	285.7	410.7
SBA	14479.4	317.6	15.85	1140.8	1480.3
LSS[a]	50.0	1.94	7.59	3.57	9.79
LSBA	241.7	2.92	5.43	0.35	0.054

[a]The abbreviation codes of LSS and LSBA were used for the leachate concentration of SS and SBA, respectively.
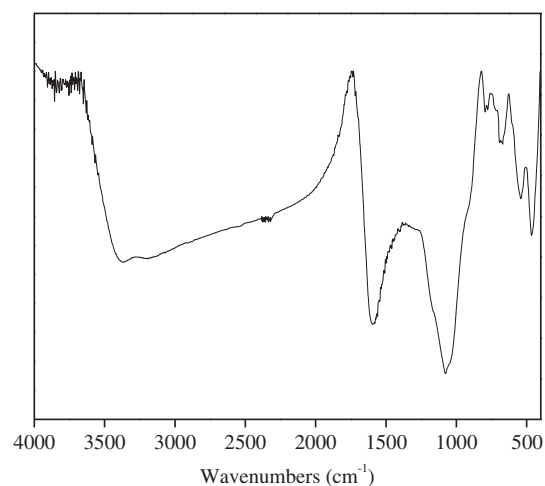

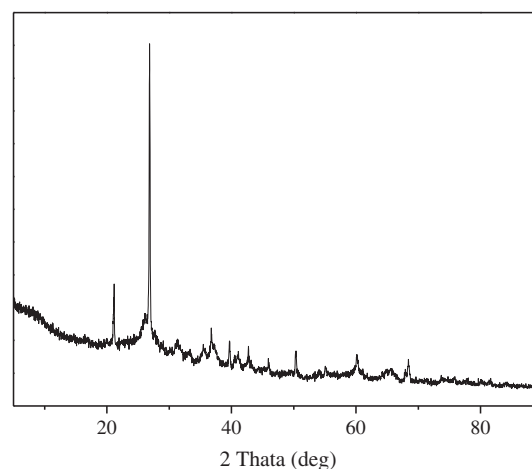Fig. 3. FT-IR spectra of SBA.

Fig. 4. XRD pattern of SBA.

organic molecules through surface complexation mechanisms [36].

XRD pattern of the SBA in Fig. 4 shows that the adsorbent had similar structure as commercial

activated carbon. Moreover, it is also noticed that quartz was the main inorganic constituent of the SBA as the result of its precursor consisting of a great deal of inorganic oxides such as SiO_2 [37].

3.2. Effect of pH

The effect of pH change and the corresponding variations in q_e are shown in Fig. 5. DMP removal was found to increase slowly between pH 2–6 (227 mg/g at maximum), then decrease slowly between pH 6–8.5, finally dropping sharply at pH 8.5–10. It can be explained that the observed effects of pH on adsorption could be related to the pH-dependent DMP and the surface charge properties of the SBA. As shown in Table 1, the dissociation constants (pK_a) of DMP were 8.59 and 11.3. Consequently, DMP molecules were predominantly neutral at pH < 8.59, with negatively charged molecules becoming dominant in the range of pH > 8.59. In addition, a pH_{PZC} value of 5.9 (shown in Table 3) for the SBA demonstrated a positive surface charge when $pH < pH_{PZC}$ and a negative surface charge when $pH > pH_{PZC}$.

Between pH 2 and 6, DMP was hydrophobic and neutral overall. As the solubility of DMP in aqueous solution was relatively low, it could be easily absorbed by an SBA containing sufficient surface adsorption sites. As shown in Fig. 5, DMP adsorption capacity was higher than 217 mg/g when the pH was between 2 and 6. In contrast, in neutral or basic aqueous solution (pH 6–8.5), the SBA surface became negatively charged, which impeded DMP adsorption to electrostatic repulsion. Furthermore, the electrostatic repulsion between anionic DMP and the SBA surface

became stronger above pH 8.5, leading to a sharp decrease in DMP removal.

3.3. Adsorption isotherms

Fig. 6 shows the DMP adsorption isotherm for distribution of the adsorbate between SBA and aqueous solution in the equilibrium state [38]. The initial slope in Fig. 6 indicates that the SBA isotherm could be classified as L-type according to Giles classification [39], suggesting that the SBA had a remarkable affinity with DMP. In addition, DMP adsorption increased continuously with an increase in its initial concentration. The maximum capacity (q_{max}) was observed to be 229 mg/g, which was higher than the reported q_{max} values for DMP adsorption of modified barium hexaferrite [40]. Furthermore, Table 6 summarizes the analysis of the two adsorption isotherm models parameters. It appeared that both the Langmuir and Freundlich equations fitted the data relatively well, as the R^2 correlation coefficients were greater than 0.9 for both models. More specifically, using the Freundlich model for DMP adsorption, the R^2 correlation coefficient was 0.9888, which was greater than that of the Langmuir model (0.9551). The Freundlich model was demonstrated to be a good model for fitting the experimental data, which may be attributed to heterogeneous distribution of active sites on the SBA's surface [41]. Since the empirical equation was assumed that the adsorption generally occurred on a heterogeneous surface or the surface of adsorbents supported sites of varied affinities, it could deduce the presence of more than one kind of adsorbent–adsorbate surface interac-
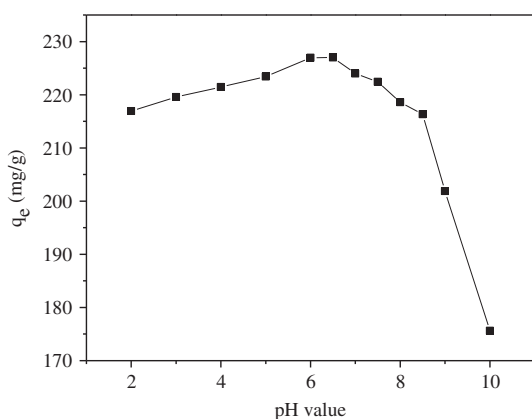

Fig. 5. Effect of pH on DMP adsorption by SBA (Initial DMP concentration is 1,000 mg/L, contact time is 2 h, adsorbent dosage is 4 g/L, pH is 2.0–10.0 and temperature is 30°C).
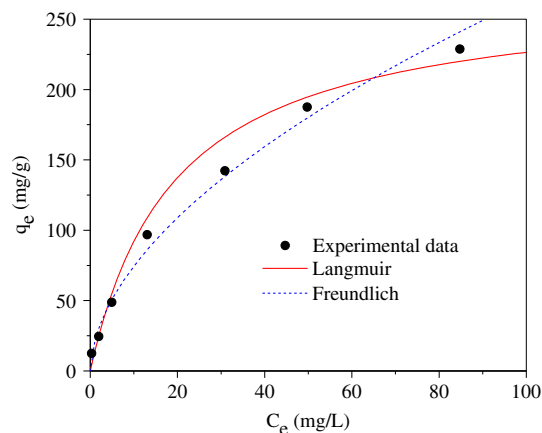

Fig. 6. Isotherm experimental data and model predictions of DMP adsorption onto SBA (Initial DMP concentration is 50–1,000 mg/L, contact time is 2 h, adsorbent dosage is 4 g/L, pH is 6.0 and temperature is 30°C).

Table 6
Langmuir and Freundlich isotherms parameters for DMP adsorption onto SBA

Langmuir		Freundlich	
q_m (mg/g)	270.27	K_f (L/mg)	20.92
K_L (L/mg)	0.0517	$1/n$	0.5505
R^2	0.9551	R^2	0.9888

Table 7
Kinetic parameters for DMP adsorption onto SBA

Pseudo-first-order	K_1 (min)	0.0222
	q_e (mg/g)	177.33
	R^2	0.9679
Pseudo-second-order	K_2 (g/mg min)	1.67×10^{-4}
	q_e (mg/g)	256.41
	R^2	0.9971
Intrapartical diffusion	K_p (mg/(g min))	12.216
	A	58.335
	R^2	0.8030

tion during adsorption process [42]. According to The Japanese Environment Agency, the adsorption process was facile when the Freundlich constant K_f and $1/n$ were between 10 and 100 mg/g, and 0.1–0.5, respectively. In this study, the calculated values for K_f and $1/n$ were 20.92 mg/g and 0.5505 (slightly high), respectively. Consequently, the experimental results reflected that DMP adsorption took place easily on the SBA.

3.4. Adsorption kinetics

Adsorption kinetics, which can provide valuable information on the adsorption mechanism in aqueous effluents, was used to investigate and describe the rate of DMP adsorption on the SBA. The DMP adsorption kinetics of the SBA at a given concentration (1,000 mg/L) is shown in Fig. 7. In addition, to monitor the adsorption kinetics, the pseudo-first-order, pseudo-second-order, and intraparticle diffusion equations were applied, with the key parameters of the three kinetic models given in Table 7.
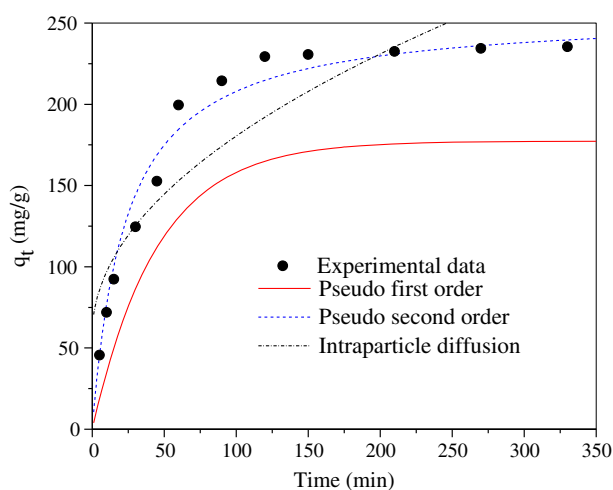

Fig. 7. Kinetic experimental data and model predictions of DMP adsorption onto SBA (Initial DMP concentration is 1,000 mg/L, contact time is 0–5.5 h, adsorbent dosage is 4 g/L, pH is 6.0 and temperature is 30°C).

The degree of agreement between the experimental data and the model predictions was determined by examining the correlation coefficients (R^2). It is well known that the higher the correlation coefficient, the lower the difference between the experimentally measured q_e and the calculated q_e. From Table 7, it is clear that both the pseudo-second-order and pseudo-first-order models fitted the experimental data, with R^2 correlation coefficients greater than 0.95 in both cases. The pseudo-second-order model appeared to be the best fit for DMP adsorption ($R^2 = 0.9971$), followed by the pseudo-first-order model ($R^2 = 0.9679$), and the intraparticle diffusion model ($R^2 = 0.8030$). The adsorption process from aqueous solution includes three stages: diffusion of the adsorbate to the adsorbent surface (external diffusion), adsorption of DMP onto surface of SBA, and diffusion through SBA pores (intraparticle diffusion) [43]. Therefore, the pseudo-second-order model is the most suitable for describing the DMP adsorption kinetics in these experiments. It indicated that the mechanism of chemical adsorption instead of the transportation of mass was the predominant rate-limiting stage of the adsorption process. In another word, the DMP adsorption rate and capacity were determined by chemical adsorption and the number of active sites occupied on the SBA, respectively [44].

3.5. Analysis of adsorption properties

As previously discussed, it was concluded that the SBA exhibited a high adsorption capacity for DMP. The high adsorption of organic contaminants was influenced not only by physical adsorption (SBA specific surface area and pore size distribution, and DMP molecular features), but also by the surface reaction between the SBA and DMP (electrostatic interactions, π–π interactions, and hydrogen bonds). Potential factors in the control of the adsorption process are discussed below.

3.5.1. Influence of pore size distribution

According to the pore-filling mechanism, the specific adsorptive interactions between adsorbent and adsorbate are associated with the adsorbate molecular size and the distribution of adsorbent pore size [44]. Pore size distribution is an important character of adsorbent, determining whether the adsorbent is able to absorb molecules of a stable size and shape. It is appropriate for microporous SBA to adsorb the pollutants in smaller size. However, the slit-shaped DMP molecule measures approximately 1.0 nm [45], and the microporous SBA exhibits a similar average pore diameter of 1.15 nm (Table 2). It is difficult for the DMP to access the SBA pores for physical adsorption. In addition, as shown in Fig. 1, SEM revealed the cylindrical pore structure of the SBA surface, which may enhance both the molecular sieving effect and the adsorption process. Thus, physical adsorption would be blocked due to the pore size distribution, as explained above. However, as an optimized DMP adsorption of 229 mg/g (>90% removal rate) was obtained in this study, it could be assumed that the adsorption process included additional adsorption mechanisms in addition to physical adsorption.

3.5.2. Influence of electrostatic interactions

Electrostatic interactions also play an important role in the high adsorption capacity of the SBA. The surface charge of the SBA and the existential state of DMP are known to change with varying pH in aqueous solution. As discussed in Section 3.2, at pH < 6, the SBA surface charge was positive, and it was assumed that neutral molecules dominate. Therefore, DMP could be easily absorbed by an SBA containing sufficient surface adsorption sites. At pH > 8.59, the SBA developed a negative surface charge, and the negatively charged DMP species became dominant. Hence, electrostatic repulsion increased with an increase in pH, thus lowering adsorption of DMP on the SBA.

3.5.3. Influence of functional groups

Previous studies demonstrated that π–π electron-donor-acceptor (EDA) interactions were the principle interactions for explaining the adsorption of aromatic hydrocarbons [46]. The molecular structure of DMP shown in Table 1 indicates the presence of an electron withdrawing carbonyl group (C=O) connected to the aromatic ring, thus rendering DMP a good π-acceptor [47]. In addition, the hydroxyl (−OH) moieties on aromatic rings (phenolic hydroxyl groups) have been demonstrated to reinforce the electron density of activated carbon graphitic planes, thus rendering the adsorbent surface as a π-donor material [31]. Furthermore, Boehm titrations (Table 4) further confirmed the presence of the phenolic hydroxyl groups (0.098 mmol/L). Hence, the influence of the phenolic hydroxyl groups resulted in the SBA being a good π-donor adsorbent, this exhibiting an excellent affinity with DMP.

Here, a possible adsorption mechanism based on hydrogen bonding interactions [48,49] was also discussed. A range of oxygen-containing functional groups on the SBA surface may therefore give different DMP adsorption capacities [48]. Hence, a number of the oxygen-containing functional groups shown in Table 4 could promote DMP adsorption by facilitating H-bond donor/acceptor interactions between DMP and the SBA surface. As can be seen in Fig. 3, a broad absorption peak between 3,500 and 3,300 cm^{-1} indicated the presence of hydroxyl groups on the SBA surface. Moreover, these hydroxyl groups are derived from phenolic hydroxyl groups and carboxyl groups, whose presence was also demonstrated by Boehm titrations (0.098 mmol/L and 0.185 mmol/g, respectively), as shown in Table 4. In addition, the molecular structure of DMP revealed the presence of carbonyl groups (C=O), as shown in Table 1, resulting in the formation of H-bonds (O–H···O) between −OH groups on the SBA surface and the C=O moiety of DMP. These intermolecular H-bonds enhanced the overall surface interactions between DMP and the SBA, which is expected to contribute to the excellent DMP adsorption affinity of the SBA.

4. Conclusion

In this study, a SBA was prepared from biochemical sludge by 3.0 M ZnCl$_2$ activation with a mass ratio of 1:1, followed by pyrolysis at 700°C for 1 h. The pore size distributions of the SBA were mainly in the micropore range, due to the caustic property of ZnCl$_2$. High carbon content and low ash amount were retained in the adsorbent following pyrolysis. The surface of the SBA was rich in acidic functional groups (−OH and −COOH). With the excellent washing procedure, the leached contents of heavy metals from SBA were low and to be acceptably safe for most industrial wastewater treatment.

The adsorption behavior of dimethyl phthalate (DMP) on the SBA was studied in batch reactors to investigate the effects of pH, DMP concentration, and adsorption time. Adsorption experiments indicated that based on the pore size distribution of the SBA, electrostatic interactions, and surface functional

groups, the SBA exhibited a remarkable adsorption capacity (227 mg/g at pH 6) for the DMP. In addition, the adsorption of the DMP on the SBA was found to follow the Freundlich isotherm. The SBA showed the heterogeneous surface supporting sites of varied affinities for the DMP adsorption. The pseudo-second-order kinetic model indicated that chemical adsorption was the predominant limiting stage during the adsorption process. We therefore successfully demonstrated that the SBA is a promising low-cost and highly effective adsorbent for the removal of DMP from aqueous solutions.

Acknowledgments

References

[1] E. Ayranci, E. Bayram, Adsorption of phthalic acid and its esters onto high-area activated carbon-cloth studied by *in situ* UV-spectroscopy, J. Hazard. Mater. 122 (2005) 147–153.

[2] J.W. Wang, F. Wang, J. Yao, R.X. Wang, H.Y. Yuan, K. Masakorala, M.M.F. Choi, Adsorption and desorption of dimethyl phthalate on carbon nanotubes in aqueous copper(II) solution, Colloids Surf. A 417 (2013) 47–56.

[3] F. Wang, J. Yao, K. Sun, B.S. Xing, Adsorption of dialkyl phthalate esters on carbon nanotubes, Environ. Sci. Technol. 44 (2010) 6985–6991.

[4] B.L. Yuan, X.T. Li, K.L. Li, W.Q. Chen, Degradation of dimethyl phthalate (DMP) in aqueous solution by UV/Si-FeOOH/H_2O_2, Colloids Surf. A 379 (2011) 157–162.

[5] P.T.C. Harrison, P. Holmes, C.D.N. Humfrey, Reproductive health in humans and wildlife: Are adverse trends associated with environmental chemical exposure? Sci. Total Environ. 205 (1997) 97–106.

[6] J.X. Mo, Z.G. Wang, W.H. Xu, S.S. Li, Z.D. Yu, Enhanced production of dimethyl phthalate-degrading strain Bacillus sp. QD_{14} by optimizing fermentation medium, Electron, J. Biotechnol. 18 (2015) 244–251.

[7] K. Pranaw, S. Singh, D. Dutta, S. Chaudhury, S. Ganguly, L. Nain, Biodegradation of dimethyl phthalate by an entomopathogenic nematode symbiont Xenorhabdus indica strain KB-3, Int. Biodeterior. Biodegrad. 89 (2014) 23–28.

[8] B. Prasad, S. Suresh, Biodegradation of dimethyl phthalate ester using free cells, entrapped cells of Variovorax sp. BS1 and cell free enzyme extracts: A comparative study, Int. Biodeterior. Biodegrad. 97 (2015) 179–187.

[9] C.F. Chang, C.Y. Man, Magnetic photocatalysts of copper phthalocyanine-sensitized titania for the photodegradation of dimethyl phthalate under visible light, Colloids Surf. A 441 (2014) 255–261.

[10] L.S. Li, W.Y. Ye, Q.Y. Zhang, F.Q. Sun, P. Lu, X.K. Li, Catalytic ozonation of dimethyl phthalate over cerium supported on activated carbon, J. Hazard. Mater. 170 (2009) 411–416.

[11] J.B. Wang, Y.R. Zhou, W.P. Zhu, X.W. He, Catalytic ozonation of dimethyl phthalate and chlorination disinfection by-product precursors over Ru/AC, J. Hazard. Mater. 166 (2009) 502–507.

[12] B.L. Yuan, X.Z. Li, N. Graham, Reaction pathways of dimethyl phthalate degradation in TiO_2-UV-O_2 and TiO_2-UV-Fe(VI) systems, Chemosphere 72 (2008) 197–204.

[13] X.K. Zhao, G.P. Yang, Y.J. Wang, X.C. Gao, Photochemical degradation of dimethyl phthalate by Fenton reagent, J. Photochem. Photobiol. A 161 (2004) 215–220.

[14] K.Y. Huang, W.L. Chou, C.T. Wang, Y.C. Chang, C.M. Shu, Electrochemically assisted coagulation for the adsorptive removal of dimethyl phthalate from aqueous solutions using iron hydroxides, J. Taiwan Instit. Chem. Eng. 50 (2015) 236–241.

[15] B. Gao, P. Wang, H.D. Zhou, Z.Y. Zhang, F.C. Wu, J. Jin, M.J. Kang, K. Sun, Sorption of phthalic acid esters in two kinds of landfill leachates by the carbonaceous sorbents, Bioresour. Technol. 136 (2013) 295–301.

[16] X.Y. Zhou, J.F. Wei, H. Zhang, K. Liu, H. Wang, Adsorption of phthalic acid esters (PAEs) by amphiphilic polypropylene nonwoven from aqueous solution: The study of hydrophilic and hydrophobic microdomain, J. Hazard. Mater. 273 (2014) 61–69.

[17] N.A. Khan, B.K. Jung, Z. Hasan, S.H. Jhung, Adsorption and removal of phthalic acid and diethyl phthalate from water with zeolitic imidazolate and metal–organic frameworks, J. Hazard. Mater. 282 (2015) 194–200.

[18] H.Y. Huang, C.L. Yang, H.X. Zhang, M.C. Liu, Preparation and characterization of octyl and octadecyl-modified mesoporous SBA-15 silica molecular sieves for adsorption of dimethyl phthalate and diethyl phthalate, Microporous Mesoporous Mater. 111 (2008) 254–259.

[19] K.M. Smith, G.D. Fowler, S. Pullket, N.J.D. Graham, Sewage sludge-based adsorbents: A review of their production, properties and use in water treatment applications, Water Res. 43 (2009) 2569–2594.

[20] E. Ayranci, E. Bayram, Adsorption of phthalic acid and its esters onto high-area activated carbon-cloth studied by *in situ* UV-spectroscopy, J. Hazard. Mater. 122 (2005) 147–153.

[21] J.D. Méndez-Díaz, M.M. Abdel daiem, J. Rivera-Utrilla, M. Sánchez-Polo, I. Bautista-Toledo, Adsorption/bioadsorption of phthalic acid, an organic micropollutant present in landfill leachates, on activated carbons, J. Colloid Interface Sci. 369 (2012) 358–365.

[22] N. Adhoum, L. Monser, Removal of phthalate on modified activated carbon: Application to the treatment of industrial wastewater, Sep. Purif. Technol. 38 (2004) 233–239.

[23] C.J. Lebigue, C. Andriantsiferana, N'G. Krou, C. Ayral, E. Mohamed, A.M. Wilhelm, H. Delmas, L. Le Coq, C. Gerente, K.M. Smith, S. Pullket, G.D. Fowler, N.J.D. Graham, Application of sludge-based carbonaceous materials in a hybrid water treatment process based on adsorption and catalytic wet air oxidation, J. Environ. Manage. 91 (2010) 2432–2439.

[24] J.L. Zou, Y. Dai, X. Wang, Z.Y. Ren, C.G. Tian, K. Pan, S. Li, M. Abuobeidah, H.G. Fu, Structure and adsorption properties of sewage sludge-derived carbon with removal of inorganic impurities and high porosity, Bioresour. Technol. 142 (2013) 209–217.

[25] G. Wen, Z.H. Pan, J. Ma, Z.Q. Liu, L. Zhao, J.J. Li, Reuse of sewage sludge as a catalyst in ozonation-Efficiency for the removal of oxalic acid and the control of bromate formation, J. Hazard. Mater. 239–240 (2012) 381–388.

[26] J.P. Reymond, F. Kolenda, Estimation of the point of zero charge of simple and mixed oxides by mass titration, Powder Technol. 103 (1999) 30–36.

[27] APHA-AWWA-WEF, Standard Methods for the Examination of Water and Wastewater, eighteenth ed., American Public Health Association, American Water Works Association, Water Pollution Control Federation, Washington, DC, 1992.

[28] Z.H. Pan, J.Y. Tian, G.R. Xu, J.J. Li, G.B. Li, Characteristics of adsorbents made from biological, chemical and hybrid sludges and their effect on organics removal in wastewater treatment, Water Res. 45 (2011) 819–827.

[29] A. Ros, M.A. Lillo-Ródenas, E. Fuente, M.A. Montes-Morán, M.J. Martín, A. Linares-Solano, High surface area materials prepared from sewage sludge-based precursors, Chemosphere 65 (2006) 132–140.

[30] G.Q. (Max) Lu, D.D. Lau, Characterisation of sewage sludge-derived adsorbents for H$_2$S removal. Part 2: Surface and pore structural evolution in chemical activation, Gas Sep. Purif. 10 (1996) 103–111

[31] J. Lladó, C. Lao-Luque, B. Ruiz, E. Fuente, M. Solé-Sardans, A.D. Dorado, Role of activated carbon properties in atrazine and paracetamol adsorption equilibrium and kinetics, Process Saf. Environ. Prot. 95 (2015) 51–59.

[32] X.N. Wang, N.W. Zhu, B.K. Yin, Preparation of sludge-based activated carbon and its application in dye wastewater treatment, J. Hazard. Mater. 153 (2008) 22–27.

[33] M.J. Martin, A. Artola, M.D. Balaguer, M. Rigola, Activated carbons developed from surplus sewage sludge for the removal of dyes from dilute aqueous solutions, Chem. Eng. J. 94 (2003) 231–239.

[34] X.G. Chen, S. Jeyaseelan, N. Graham, Physical and chemical properties study of the activated carbon made from sewage sludge, Waste Manage. 22 (2002) 755–760.

[35] O. Duggan, S.J. Allen, Study of the physical and chemical characteristics of a range of chemically treated, lignite based carbons, Water Sci. Technol. 35 (1997) 21–27.

[36] O. Gulnaz, A. Kaya, S. Dincer, The reuse of dried activated sludge for adsorption of reactive dye, J. Hazard. Mater. 134 (2006) 190–196.

[37] G.Q. Lu, J.F. Low, C.Y. Liu, Surface area development of sewage sludge during pyrolysis, Fuel 74 (1995) 244–248.

[38] M.R. Malekbala, M.A. Khan, S. Hosseini, L.C. Abdullah, T.S.Y. Choong, Adsorption/desorption of cationic dye on surfactant modified mesoporous carbon coated monolith: Equilibrium, kinetic and thermodynamic studies, J. Ind. Eng. Chem. 21 (2015) 369–377.

[39] X.Y. Ge, F. Tian, Z.L. Wu, Y.J. Yan, G. Cravotto, Z.S. Wu. Adsorption of naphthalene from aqueous solution on coal-based activated carbon modified by microwave induction: Microwave power effects, Chem. Eng. Process. 91 (2015) 67–77.

[40] B. Osman, E.T. Özer, A. Kara, Ş. Güçer, N. Beşirli, Assesment of dimethyl phthalate removal from aqueous phase using barium hexaferrite containing magnetic beads, J. Colloid Interface Sci. 378 (2012) 167–174.

[41] I.A.W. Tan, A.L. Ahmad, B.H. Hameed, Adsorption isotherms, kinetics, thermodynamics and desorption studies of 2,4,6-trichlorophenol on oil palm empty fruit bunch-based activated carbon, J. Hazard. Mater. 164 (2009) 473–482.

[42] A. Bahdod, S. El Asri, A. Saoiabi, T. Coradin, A. Laghzizil, Adsorption of phenol from an aqueous solution by selected apatite adsorbents: Kinetic process and impact of the surface properties, Water Res. 43 (2009) 313–318.

[43] F. Rozada, M. Otero, A. Morán, A.I. García, Activated carbons from sewage sludge and discarded tyres: Production and optimization, J. Hazard. Mater. 124 (2005) 181–191.

[44] X.N. Li, S. Chen, X.F. Fan, X. Quan, F. Tian, Y.B. Zhang, J.S. Gao, Adsorption of ciprofloxacin, bisphenol and 2-chlorophenol on electrospun carbon nanofibers: In comparison with powder activated carbon, J. Colloid Interface Sci. 447 (2015) 120–127.

[45] A. Rossner, S.A. Snyder, D.R.U. Knappe, Removal of emerging contaminants of concern by alternative adsorbents, Water Res. 43 (2009) 3787–3796.

[46] L.L. Ji, F.L. Liu, Z.Y. Xu, S.R. Zheng, D.Q. Zhu, Adsorption of pharmaceutical antibiotics on template-synthesized ordered micro- and mesoporous carbons, Environ. Sci. Technol. 44 (2010) 3116–3122.

[47] Q.S. Liu, T. Zheng, P. Wang, J.P. Jiang, N. Li, Adsorption isotherm, kinetic and mechanism studies of some substituted phenols on activated carbon fibers, Chem. Eng. J. 157 (2010) 348–356.

[48] D.J. de Ridder, L. Villacorte, A.R.D. Verliefde, J.Q.J.C. Verberk, S.G.J. Heijman, G.L. Amy, J.C. van Dijk, Modeling equilibrium adsorption of organic micropollutants onto activated carbon, Water Res. 44 (2010) 3077–3086.

[49] I. Villaescusa, N. Fiol, J. Poch, A. Bianchi, C. Bazzicalupi, Mechanism of paracetamol removal by vegetable wastes: The contribution of π–π interactions, hydrogen bonding and hydrophobic effect, Desalination 270 (2011) 135–142.